Journal of
Manufacturing and Materials Processing

MDPI

Article

Machining-Induced Burr Suppression in Edge Trimming of Carbon Fibre-Reinforced Polymer (CFRP) Composites by Tool Tilting

Tamás Sándor Tima and Norbert Geier *

Department of Manufacturing Science and Engineering, Faculty of Mechanical Engineering, Budapest University of Technology and Economics, Műegyetem rkp. 3., 1111 Budapest, Hungary
* Correspondence: geier.norbert@gpk.bme.hu; Tel.: +36-1-463-2641

Abstract: Several challenges arise during edge trimming of carbon fibre-reinforced polymer (CFRP) composites, such as the formation of machining-induced burrs and delamination. In a recent development, appropriate-quality geometric features in CFRPs can be machined using special cutting tools and optimised machining parameters. However, these suitable technologies quickly become inappropriate due to the accelerated tool wear. Therefore, the main aim of our research was to find a novel solution for maintaining the machined edge quality even if the tool condition changed significantly. We developed a novel mechanical edge-trimming technology inspired by wobble milling, i.e., the composite plate compression is governed by the proper tool tilting. The effectiveness of the novel technology was tested through mechanical machining experiments and compared with that of conventional edge-trimming technology. Furthermore, the influences of the tool tilting angle and the permanent chamfer size on the burr characteristics were also investigated. A one-fluted solid carbide end mill with a helix angle of 0° was applied for the experiments. The machined edges were examined trough stereomicroscopy and scanning electron microscopy. The images were evaluated through digital image processing. Our results show that multi-axis edge-trimming technology produces less extensive machining-induced burrs than conventional edge trimming by an average of 50%. Furthermore, we found that the tool tilting angle has a significant impact on burr size, while permanent chamfer does not influence it. These findings suggest that multi-axis edge trimming offers a strong alternative to conventional methods, especially when using end-of-life cutting tools, and highlight the importance of selecting the optimal tool tilting angle to minimize machining-induced burrs.

Keywords: CFRP; edge trimming; burr; tool tilting; digital image processing

Citation: Tima, T.S.; Geier, N. Machining-Induced Burr Suppression in Edge Trimming of Carbon Fibre-Reinforced Polymer (CFRP) Composites by Tool Tilting. *J. Manuf. Mater. Process.* **2024**, *8*, 247. https://doi.org/10.3390/jmmp8060247

Academic Editor: Yusheng Shi

Received: 7 October 2024
Revised: 31 October 2024
Accepted: 3 November 2024
Published: 5 November 2024

1. Introduction

Carbon fibre-reinforced polymer (CFRP) composites are widely applied and will be spread further in high-end industries such as the aerospace and automobile industries, mainly due to their easy-to-shape behaviour and excellent specific mechanical properties [1]. Although these fibrous composites are often manufactured almost ready to shape using automated composite manufacturing technologies [2], complex geometric features (i.e., difficult to mould and laminate) are often post-manufactured by mechanical machining technologies such as drilling or edge trimming [3]. CFRPs are considered to be difficult-to-cut materials mainly because the carbon fibre reinforcements have high resistance against cutting and can easily be buckled, resulting in accelerated tool wear and burrs, and have significant abrasive wear effects on the cutting tool, resulting in more machining-induced geometrical defects (delamination, burrs, fibre pull-out, matrix burning, etc.). Furthermore, the process planning and optimisation of the machining technology and the prediction of quality are challenging because of the inhomogeneity and anisotropy of the CFRP composites [4].

A considerable extent of machining-induced burrs is risky and not allowed because of the dimensional distortion of the part edge, assembly challenges and the potential for the burr to serve as a starting point for further damage propagation [5]. David et al. [6] pointed out that the costs associated with removing burrs in the aerospace industry can be up to 30% of manufacturing costs. Therefore, this study focussed on the analysis and suppression of such machining-induced burrs. Although the ISO 13715:2017 standard defines burr height as a characteristic of machining-induced burrs on the machined edges of metallic parts, this approach often cannot be implemented directly for the proper characterisation of burrs in fibrous composites. Researchers apply numerous parameters (e.g., burr height, burr width, burr factor and contour burr factor) describing burrs in fibrous composites, depending mainly on the analysed geometrical feature and related application [7–9].

Edges of high-end CFRP composite parts that will later be assembled must often be machined to meet strict dimensional requirements without burrs [10]. Mechanical edge trimming is one of the most common machining technologies applied to CFRPs [10–12]. Although considerable efforts have been made in the technology improvement and optimisation of non-traditional edge-trimming technologies such as abrasive water jet cutting [13], laser beam cutting [14], electro-discharge machining [15], laser scored machining [16] etc., numerous difficulties still arise during their industrial implementation. Conventional mechanical edge trimming (i.e., the axis of the end mill is parallel to the machined surface) using advanced end mill geometries (e.g., the compression end mill and the honeycomb end mill) is easy to implement and can produce excellent quality edges on CFRPs until the accelerated tool wear significantly changes the tool condition (i.e., increases the cutting edge radius—CER) and results in inappropriate chip removal [17].

Su et al. [18] conducted experiments with conventional mechanical edge trimming of CFRPs and found that the depth of the cut has a significant effect on chip formation. Schorník et al. [19] conducted edge-trimming experiments with CFRPs and investigated the influence of the cutting conditions on the quality of the machined surfaces. They determined that the optimal feed rate for the given cutting speed (502.4 m/min) was 200 mm/min. Pecat et al. [20] investigated the influence of milling process parameters on the surface integrity of CFRPs. They found that, regarding the fibre orientation, a smooth surface was found for milling at fibre cutting angles (Θ—the angle between the cutting speed and fibre direction) of 0° and +45°; however, at −45° and 90°, some of the micrographs showed severe damage in the form of cracks and segmentation. Yashiro et al. [21] investigated the temperatures of the cutting tool and machined surface layer in the milling of CFRPs. Based on their experiments, the measured temperature at the tool–workpiece contact point reached 180 °C at a cutting speed of 25 m/min and then exceeded the glass-transition temperature at a cutting speed higher than 50 m/min. The researchers agreed that the fibre cutting angle plays an essential role in chip removal and defect formation mechanisms, as do the cutting strategy (i.e., up or down milling) and cutting edge condition (cutting edge radius, rake angle, friction properties, etc.). Geier [22] conducted up and down milling experiments in unidirectional CFRP, investigating how the cutting direction affects the cutting force. He found that the smallest cutting force occurred at a fibre cutting angle of 120°, as was also found by Liu et al. [23]. Zhang et al. [24] studied the high-speed up and down milling of unidirectional CFRP material with varied fibre orientation angles. They concluded that the cutting speed has a significant impact on the milling force during the machining of unidirectional CFRP composites. Zhenyuan et al. [25] experimentally analysed the effects of temperature on the milling of multi-directional CFRP composites, and the mechanism for cutting laminated layers with different fibre orientations was revealed under different temperatures. They concluded that jetting cryogenic nitrogen gas at different distances is an effective way to control the cutting-area temperature in end milling of CFRP composites. The temperature drops from 135 °C without coolant to as low as −50 °C by applying the cooling gas at a close distance. Additionally, the temperatures generally reach a similar level as long as the cooling operations are conducted at the same distance. Li et al. [26] proposed a new cutting force control method called “cutting width

discretization" based on the effect of effective cutting-edge length on the material removal process when cutting CFRP laminates with a ball-end milling cutter. Based on the new cutting force control method, they concluded that the milling force of the ball-end milling cutter for CFRP laminates can be reduced by reasonably reducing the volume of cutting material per tooth.

Considerable efforts have been made in the investigation of slot-milling-induced burrs in CFRPs. The experiences gained through slot milling can be adapted to the development of edge-trimming technologies; thus, these experiences are worth considering. Jamal et al. [27] investigated the cutting forces occurring during slot milling. It was found that damage caused by machining was greatest when the resulting shear force was sufficiently large compared to the strength of the transverse reinforcing fibres. El-Hofy et al. [28] investigated the temperature of the tool during slot milling. Their research revealed that the highest temperature occurred at a fibre cutting angle of 45°. Ziyang et al. [29] studied the milling force and surface quality during slot milling. They found that an increase in the tool rake angle has no obvious effect on surface roughness. However, the surface roughness is affected by the equivalent cutting area because the material-removal mechanism and failure form are different for different equivalent cutting areas. Haifeng et al. [30] developed a prediction model for the milling of multi-directional CFRP laminate. The model considers the effects of instantaneous uncut chip thickness, fibre cutting angle, spindle speed and axial depth of cut. They found that the unidirectional CFRP laminate milling force model could be successfully extended to the prediction of multidirectional CFRP laminate milling force by superposition theory. Experiments proved that the predicted results were in good agreement with the experimental results.

Multi-energy field-assisted machining is a new and emerging machining technology that uses multiple energy sources to improve material removal processes. The technique involves the combined use of several types of energy (electrical, magnetic, ultrasonic, etc.) to increase machining efficiency or machining accuracy [31,32]. For example, Zheng et al. [33] focused on optimising the laser parameters during CFRP machining. They concluded in their research that issues such as fibre pull-out and interlayer delamination occur during processing due to the anisotropic and complex structure of CFRPs. In their future research, they will focus on more intelligent laser cutting systems to achieve high-quality, high-efficiency CFRP processing.

The cutting conditions during edge trimming can be improved not only by using advanced tool geometries, optimised process parameters, energy field-assisted technologies and cooling [34–39] but also by effective tool motion [40,41]. Conventional tool motion can be complemented by the appropriate manipulation of a tool's tilting angle. Although the tilting of the tool is currently costly to implement in the industry (it requires control of five independent axes of machine tools or industrial robots), a few attempts have already been made to investigate the influence of the tool tilting on the machining-induced geometrical defects in CFRPs. Hosokawa et al. [42] conducted edge-trimming experiments in CFRP with a high-helix end mill and tool tilting. They found that the proper tool tilting (i.e., tilting such that the resultant cutting force acted parallel to the composite surface) resulted in reduced tool wear and improved surface integrity. Schulze et al. [43] machined the CFRP composite with wobble milling technology. This technology enables the machining of the workpiece's top layers, with the resulting process force vector being significantly directed toward the centre of the workpiece. Schulze et al. [44] compared several hole machining technologies in their research, including wobble milling. They found that wobble milling resulted in the least damage during the machining. Hintze et al., in their work [45], developed a three-dimensional description of the geometrical and kinematic relationships involved in wobble milling. Based on their research, it can be concluded that fibre protrusion can be avoided if the cutting speed is at least partially directed in the following direction in the plane of the plywood and if the cutting edge is partly above the fibre to be cut. Pereszlai et al. [46] investigated wobble milling using three types of cutting tools. They found that the tool type has a significant effect on the burr factor. Compared

with other hole machining technologies, all of the analysed tools produced better-quality holes when wobble milling was used than when conventional or helical milling was used.

Reflecting on the above-discussed deficiencies and challenges of mechanical edge trimming of CFRPs, the main aim of the present study is to develop a novel strategy to minimise edge-trimming-induced burrs on the machined edges of CFRP plates. Therefore, we developed a complex, tilted edge trimming technology (i.e., multi-axis technology), presented in Section 2. The novel technology was tested through machining experiments and compared with conventional edge trimming, as described in Section 3. Finally, the experimental results are presented and discussed in Section 4.

2. Description of the Novel Multi-Axis Edge-Trimming Technology

The novel edge-trimming technology is inspired by five-axis wobble milling technology that is capable of excellent-quality hole machining in fibrous composites [46]. The main advantage of wobble milling lies in the proper control of the cutting force, resulting in a compression effect and thus in the minimisation of machining-induced geometrical defects. We adapted this advanced hole-machining technology to edge trimming by the linear expansion of wobble milling. Considering that the cutting force is controlled mainly by the tool inclination (i.e., tool tilting) in the proposed novel technology, conventional milling tools should also be able to produce suitable-quality machined surfaces on CFRPs, not only advanced (i.e., expensive) end mills such as honeycomb end mills. In addition, we expect that the quality of the machined edges is more easily maintainable even with accelerated tool wear if the layers are properly compressed by the novel technology.

The developed multi-axis edge trimming operation is constructed as follows. In the first step, the conventional tool machines a ($c + a_{ef}$ (mm) x φ (°)) chamfer on one side of the CFRP composite edge, as illustrated in Figure 1a. In the first step, the technology removes area I (triangle AEB), which is shown in Figure 2. Although this cutting movement does not require a five-axis interpolation, the positioning of the cutting tool requires rotating axes. Figure 1d illustrates that the cutting force compresses the top CFRP layers while the tilted tool machines the chamfer because the radial cutting force component is perpendicular to the chamfer surface. As long the cutting force compresses the outer fibres to the inner CFRP layers, the outer fibres are mechanically supported against buckling, resulting in a proper cut. This compression effect is advantageous from the point of view of machining-induced burr and delamination formation. Furthermore, the chip cross-section at the final edge geometry is negligible; thus, the probability of chip-cross-section-dependent burr and delamination formation is expected to be low as well. Then, the first step is repeated at the other side of the CFRP composite plate (Figure 1b) to prepare a symmetrical CFRP plate for the finishing movement. In the second step, the technology removes area II (triangle A'E'B'), as shown in Figure 2. This figure shows that the novel technology has to remove three areas of rest material (I, II and III), and the first and second steps' area of rest material is identical. Finally, the rest of the material (area III, i.e., quadrilateral BDD'B' in Figure 2) is removed by the cutting tool as it is tilted perpendicularly relative to the normal ($\underline{n}$) of the surface of the final machined CFRP edge (Figure 1c).

The algorithm of the developed edge trimming technology is shown in Figure 3, supporting the implementation of the main steps of the developed multi-axis edge trimming operation. Considering that the presented algorithm is independent of the CNC controller and kinematics of the machine tool, a five-axis indexing operation is required before each feed movement to provide the required tool positions. However, based on the nominal position of the tool axis and the orientation of the CFRP plate, the coefficients of the indexing in the real environment have to be determined, respectively.

The developed multi-axis technology was compared with a conventional milling technology. Conventional technology removes the rest material in a single step and does not favourably compress the edge of CFRP composites. The applied conventional edge-trimming technology is illustrated in Figure 4.

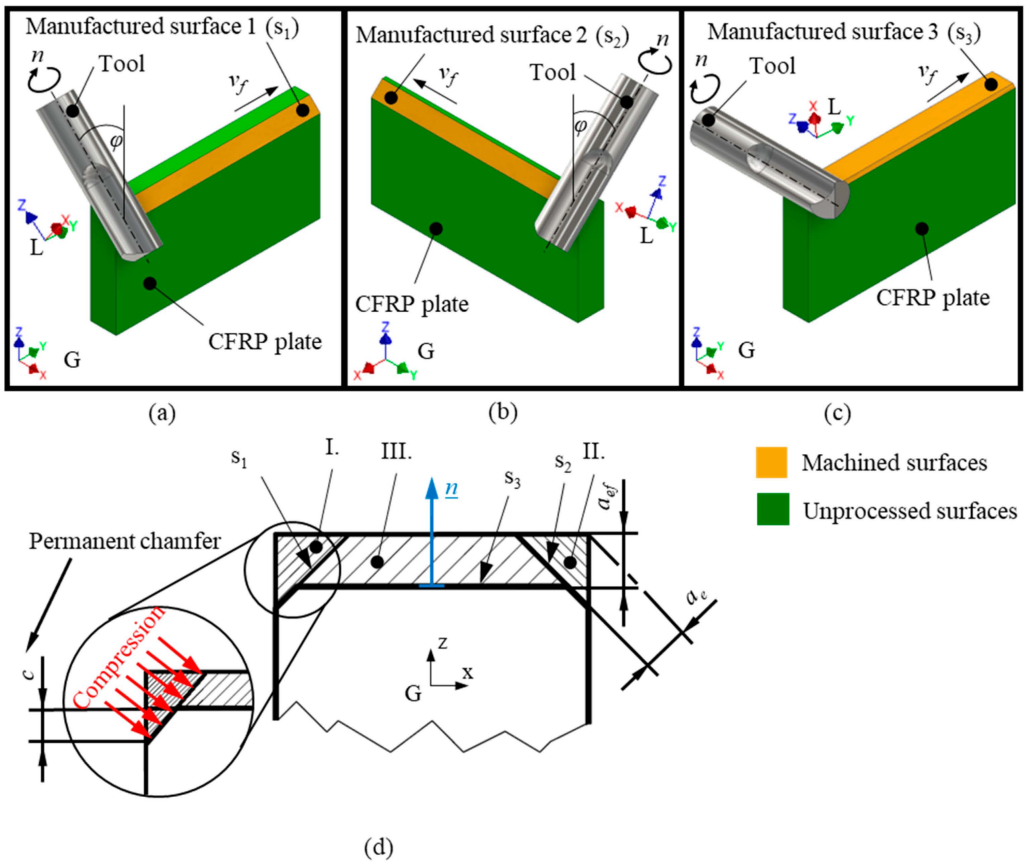

Figure 1. Illustration of the main steps of the novel edge-trimming technology: (**a**) chamfer machining on one of the edges; (**b**) chamfer machining on the other side of the plate, (**c**) the finishing step of the multi-axis technology and (**d**) an illustration of the compression effect, where a_{ef} is the cutting width in the final step, a_e denotes the cutting width of the tilting steps, v_f is the feed rate, φ is the tool tilting angle, n is the spindle speed, c is the permanent chamfer size, $\underline{n}$ is the normal of the final machined CFRP edge surface, G is the global coordinate system fixed to the machine tool and L is the local coordinate system fixed to the end mill.

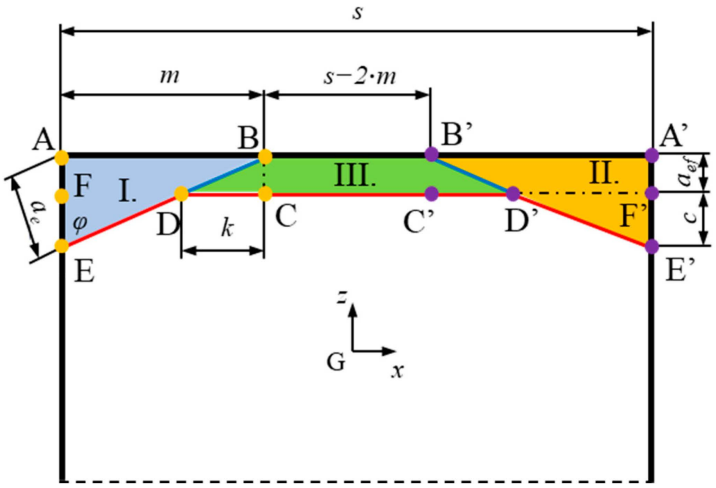

Figure 2. Illustration of a cross section of the multi-axis technology, where the area I is removed first, followed by the area II and the area III respectively.

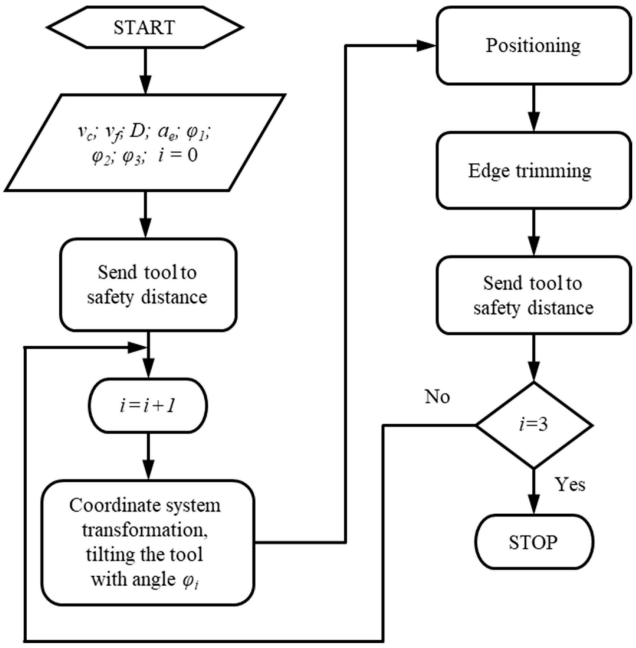

Figure 3. The algorithm of the developed multi-axis mechanical edge-trimming technology, where v_c denotes the cutting speed, v_f is the feed rate, D is the tool diameter, a_e is the width of the cut, φ_i is the tool tilting angle for the ith cutting step and i is a running parameter.

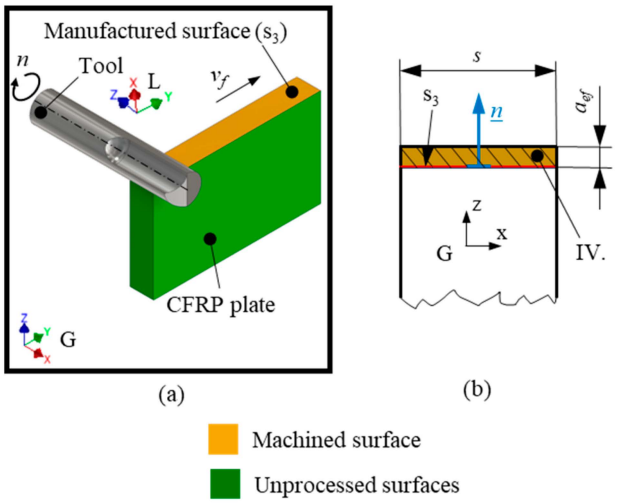

Figure 4. (**a**) Illustration of conventional machining technology, where a_{ef} denotes the cutting width, v_f is the feed rate, n is the spindle speed, $\underline{n}$ is the normal of the final machined CFRP edge surface, G is the global coordinate system and L is the local coordinate system; (**b**) illustration of allowance plan.

3. Experimental Setups and Methods

3.1. Materials, Tools and Equipment

Experiments in mechanical edge trimming were performed in unidirectional carbon fibre-reinforced vinyl ester composites having a nominal plate thickness of 5 mm. The CFRP plate was purchased from one of our industrial partners, who wishes to remain anonymous. However, the key material properties of the CFRP plate were measured and published in Ref. [47]. The purchased composite plate was cut into smaller CFRP specimens (Figure 5c) having a nominal size of 35 × 22 × 5 mm to meet the requirements of the applied machining fixture and working-space limitations. The cutting was conducted on a Mutronic Diadisc 5200 (manufacturer: MUTRONIC Präzisionsgerätebau GmbH & Co. KG, city: Rieden, country: Germany) cutting machine.

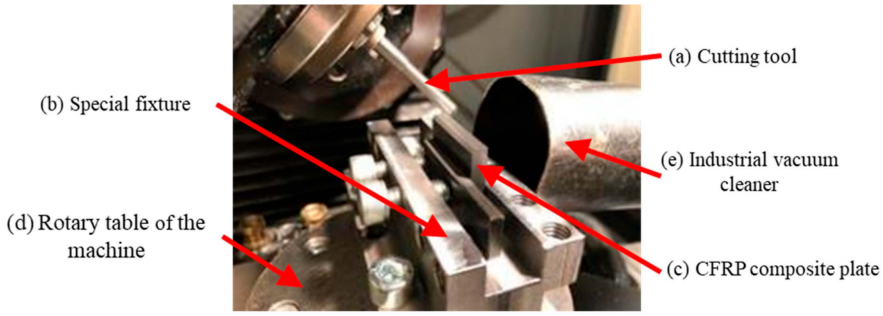

Figure 5. Experimental setup: (**a**) cutting tool, (**b**) special fixture, (**c**) CFRP composite plate, (**d**) rotary table of the machine tool and (**e**) industrial vacuum cleaner.

The edge-trimming experiments were conducted on a VHTC−130 LINEAR (manufacturer: NCT, city: Budapest, country: Hungary) five-axis machining centre having three linear axes (X, Y and Z), a rotary table (C axis) and a tilting spindle head (B axis). Therefore, the composite was fixed to the rotary table, and the spindle head provided the tool tilting angle of φ and permanent chamfer size of c.

A THOMAS 23N1106 (manufacturer: FFDM TIVOLY, city: Bourges, country: France) uncoated carbide milling tool was applied, having a diameter of 6 mm, a helix angle of 0° and only one cutting edge (Figure 5a). A special fixture was used to fix the CFRP composite (Figure 5b). The experiments were carried out under dry conditions. The chips were evacuated from the cutting zone with a Nilfisk GB733 (manufacturer: Nilfisk A/S, city: Copenhagen, country: Denmark) industrial vacuum cleaner (Figure 5e) having a rated power of 1.85 kW and nominal airflow of 86 L/s. The experimental setup can be seen in Figure 5.

After the milling experiments, we examined the quality of the machined edges of the CFRP composites with an OLYMPUS SZX16 (manufacturer: Olympus Europa SE & Co. KG, city: Hamburg, country: Germany) stereomicroscope. We captured the machined edges from the direction of the normal of the machined edge (vector $\underline{n}$, as illustrated in Figure 1), with a resolution of 2448 × 1920 pixels and a nominal magnification of 20× . These raw images were further processed using digital image processing, as presented in Section 3.3. A Zeiss Evo MA 10 (manufacturer: Carl Zeiss AG, city: Jena, country: Germany) scanning electron microscope was used to characterise the microgeometry and thereby the quality of representative machined edges at 100×, 200 × and 2750× magnification.

3.2. Experimental Design

We designed the mechanical-edge-trimming experiments to evaluate the performance of the developed multi-axis edge-trimming technology relative to conventional edge trimming. The feed rate (v_f), cutting width (a_e) and machining strategy (S) were selected as factors. The factor levels were set using Minitab 21.4.0 software based on the Central Composite Circumscribed (CCC) design. The feed rate and the cutting width varied across five levels each, while the manufacturing technology varied across two levels. The experimental factors and levels are summarized in Table 1. In the centre of the factor space, the experiments were repeated five times to determine the reproducibility characteristics. To deal with systematic errors, the experiments were performed in a random order. The spindle speed (n = 6000 rpm, i.e., cutting speed of v_c = 113.04 m/min) and the tool tilting angles ($\varphi_1 = 45°$, $\varphi_2 = -45°$ and $\varphi_3 = 90°$) were fixed. The orientation of the carbon fibres was perpendicular to the direction of the feed rate. All individual allowance shapes were removed in one pass. The tilting cutting width (a_e) was equal to the final cutting width (a_{ef}).

In addition to the experiments presented above (Table 1), we designed another mechanical-edge-trimming experiment to analyse the multi-axis edge-trimming technology in more detail. The tool tilting angle (φ) and the permanent chamfer size (c) were selected as factors and varied systematically according to the CCC design (Table 2). In the centre of the factor space, the experiments were repeated five times to determine the reproducibility

characteristics. To deal with systematic errors, the experiments were performed in a random order. The spindle speed (n = 6000 rpm, i.e., cutting speed of v_c = 113.04 m/min), the feed rate (v_f = 200 mm/min) and the cutting width in the final step (a_{ef} = 0.5 mm) were fixed. The orientation of the carbon fibres was perpendicular to the feed direction. All individual allowance shapes were removed in one pass. No coolant was used during cutting.

Table 1. Factors and levels to analyse the effects of feed rate, cutting width and manufacturing technology.

Factors		Levels				
		1	2	3	4	5
Feed rate	v_f (m/min)	100.000	143.934	250.000	356.066	400.000
Cutting width	a_e (mm)	0.300	0.343	0.450	0.556	0.600
Manufacturing technology	S (-)	conventional (C)	multi-axis (T)			

Table 2. Factors and levels to analyse the effects of tool tilting angle and permanent chamfer size.

Factors		Levels				
		1	2	3	4	5
Tool tilting angle	φ (°)	10.000	20.251	45.000	69.749	80.000
Permanent chamfer size	c (mm)	0.000	0.073	0.250	0.427	0.500

3.3. Applied Methods

The digital images taken with the stereomicroscope were first segmented and inverted; then, the number of white pixels in the binarized images was counted. Considering that the machined edges could not be precisely positioned parallel to the horizontal axis of the microscope, the images had to be rotated. Using the least squares method, we first fitted a straight line (coloured red in Figure 6) to the white pixels of the binary edge.

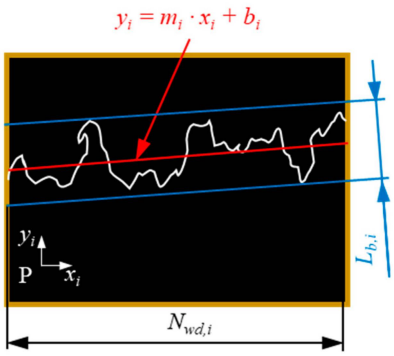

Figure 6. Illustration of the maximum burr size, where $N_{wd,i}$ (-) is the width of the image, $L_{b,i}$ (µm) is the average burr length, y_i is the equation of a straight line fitted by the method of least squares, m_i is the slope of the fitted line and P denotes the coordinate system fixed to the captured images.

The maximum burr size (L_b) metric was inspired by the ISO 13715:2017 standard and roughness depth (Rz) metric (ISO 4288:1996 standard) used during the surface roughness evaluation. The distance from the baseline (red colour in Figure 6) was determined in the positive and negative directions. The absolute value of the minimum was added to the maximum value to obtain the maximum burr size. The maximum burr size was calculated as expressed by Equations (1) and (2) and illustrated in Figure 6.

$$y'_{Nwh,i,j} = (y_{N_{wh,i,j}} - y_i) \cdot \cos(\text{arctg}(m_i)) \quad (1)$$

$$L_b = \frac{1}{n}\sum_{i=1}^{n}\left(\max\left(y'_{Nwh,i,j}\right) + \left|\min\left(y'_{Nwh,i,j}\right)\right|\right) \cdot \frac{s_{\mu m}}{s_{pixel}} \quad (2)$$

where L_b (µm) is the maximum burr size, $y_{Nwh,i}$ (-) are the "y" coordinates of the white pixels, $y'_{Nwh,i}$ (-) are the distance between the white pixel and the straight line, y_i is the equation of the straight line, m_i is the slope of the fitted (red) line, n is the number of images taken, $s_{\mu m}$ (µm) is the scale in µm and s_{pixel} (pixels) is the scale in pixels.

The specific average edge length (L_e) was calculated from the slope (m_i) of the fitted (red) line and the width ($N_{wd,i}$) of the created image based on Equations (3) and (4). Since three images were taken of each edge, the specific average edge lengths were obtained by averaging the obtained specific average edge lengths (L_e). The compensation is illustrated in Figure 7.

$$L_{y,i} = \frac{N_{wd,i}}{\cos(\text{arctg}(m_i))} \tag{3}$$

$$L_e = \frac{1}{n}\sum_{i=1}^{n}\frac{N_{wh,i}}{L_{y,i}} \tag{4}$$

where L_e (-) is the specific average edge length, $L_{y,I}$ (-) is the length of the fitted straight line, $N_{wh,i}$ (-) is the number of white pixels, $N_{wd,i}$ (-) is the width of the image, m_i is the slope of the fitted (red) line and n is the number of images taken. The parameters L_b and L_e were both applied to characterise the quality of the machined edges.

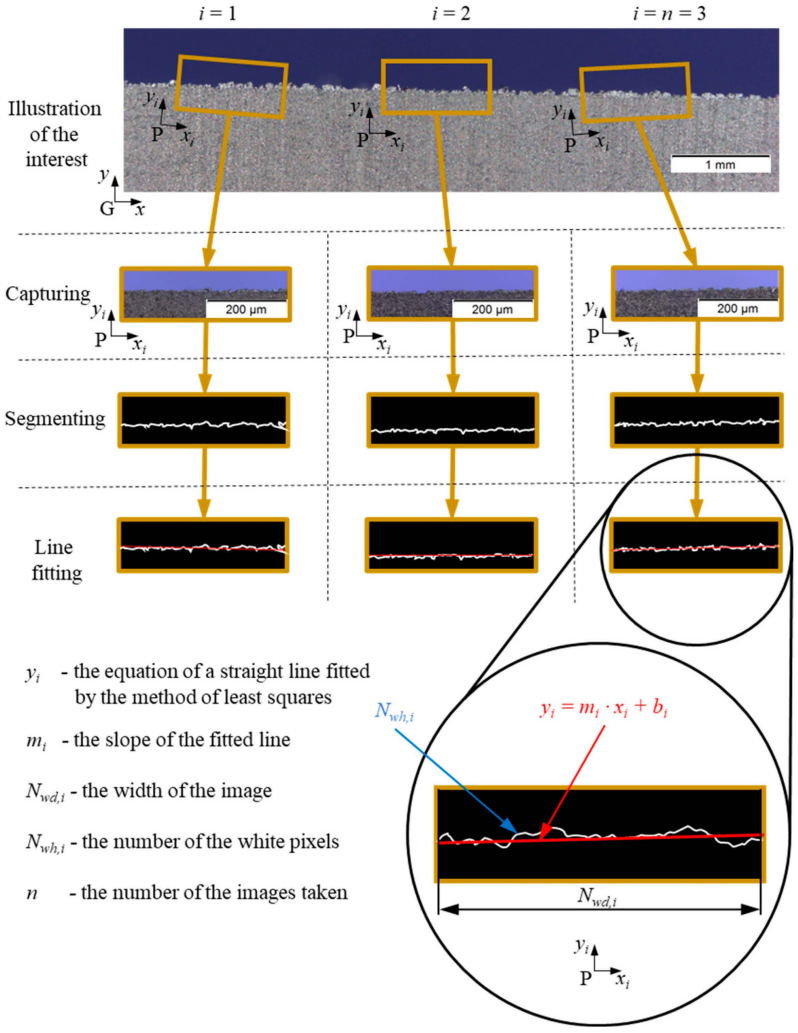

Figure 7. Illustration of the compensation, where $N_{wh,i}$ is the number of white pixels, $N_{wd,i}$ is the width of the image and n is the number of images taken.

4. Results and Discussion

The experimental results of the analysis on the influences of the feed rate, cutting width and strategy (Table 1) are presented in Section 4.1, and the results of the analysis on the influences of the tool tilting angle and permanent chamfer size are presented in Section 4.2, while the findings and outlook are discussed in Section 4.3.

4.1. Influence of the Feed Rate, Cutting Width and Strategy

The experimental runs, factor levels and corresponding calculated response values (L_e and L_b) are summarised in Table 3. Figure 8 shows the raw (unprocessed) images of the machined edges. The numerical results in the table and the unprocessed images clearly indicate that the conventional (*C*) technology resulted in significantly larger burrs than the novel multi-axis (*T*) technology, which is very promising.

Table 3. Experimental runs, factor levels and calculated response values.

Experiment Number	Factors			Response Values	
	Feed Rate	Cutting Width	Strategy	Specific Average Edge Length	Maximum Burr Size
No. (-)	v_f (mm/min)	a_e (mm)	*S* (-)	L_e (-)	L_b (µm)
1	143.934	0.556	*C*	1.779	18.929
2	143.934	0.556	*T*	1.239	10.407
3	250.000	0.450	*C*	2.195	4.496
4	250.000	0.450	*T*	1.309	7.986
5	250.000	0.450	*C*	2.219	24.507
6	250.000	0.450	*T*	1.617	9.207
7	143.934	0.343	*C*	2.837	22.729
8	143.934	0.343	*T*	1.541	3.999
9	100.000	0.450	*C*	1.584	15.343
10	100.000	0.450	*T*	1.579	11.379
11	250.000	0.450	*C*	2.371	28.495
12	250.000	0.450	*T*	1.503	8.309
13	250.000	0.450	*C*	2.031	21.538
14	250.000	0.450	*T*	1.318	14.766
15	250.000	0.600	*C*	2.189	32.728
16	250.000	0.600	*T*	1.280	13.242
17	356.066	0.343	*C*	1.309	16.274
18	356.066	0.343	*T*	1.289	10.123
19	250.000	0.300	*C*	1.309	10.431
20	250.000	0.300	*T*	1.318	8.537
21	250.000	0.450	*C*	1.373	14.218
22	250.000	0.450	*T*	1.343	8.335
23	356.066	0.556	*C*	1.511	25.386
24	356.066	0.556	*T*	1.381	8.595
25	400.000	0.450	*C*	1.811	25.420
26	400.000	0.450	*T*	1.501	14.013

The main effect diagram of the edge-trimming technology is shown in Figure 9. The expected (nominal) value of the specific edge length of conventionally machined edges was significantly larger than that of edges machined by the multi-axis technology. The difference between the two technologies was 0.48. Based on the ANOVA results, the interaction terms of the machined technology were not significant at a significance level of 0.05, as shown in Table 4(a). The standard deviation was larger in the case of conventionally machined edges. Considering that the upper and lower layers of the composite plate are not compressed during conventional milling, the edge quality is expected to be worse than that of multi-axis edge trimming. The main effect diagram of the maximum burr size is shown in Figure 9b. It correlates with the main effect diagram of the specific average edge length. The maximum burr size of the edges machined with multi-axis technology was

significantly smaller. The difference between the two technologies was 13.818 µm. This was confirmed by the ANOVA table for maximum burr size (Table 4(b)).

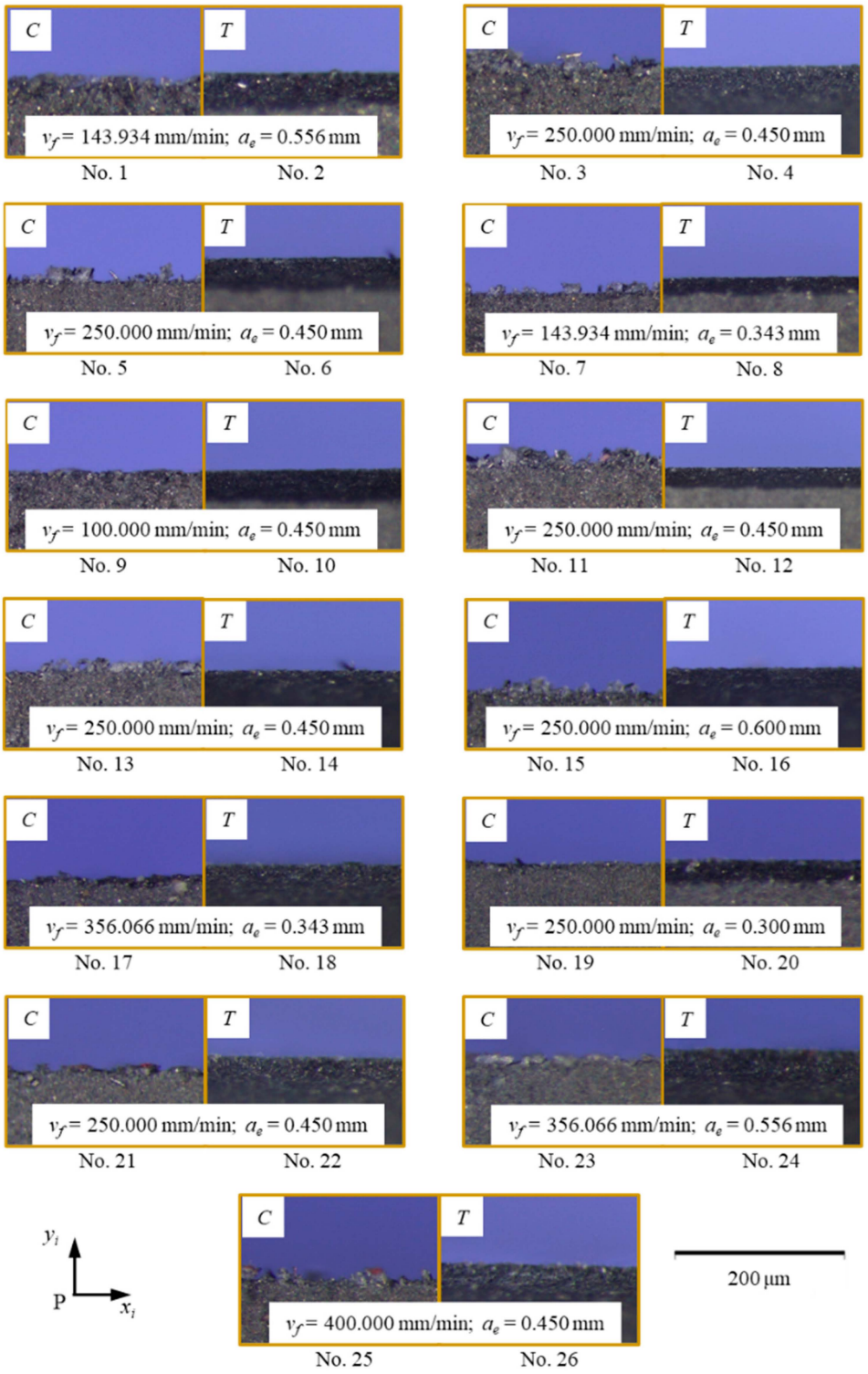

Figure 8. Raw images of the machined edges of the CFRP composites, where the *C* denotes the conventional and *T* denotes the multi-axis (tilted) strategy.

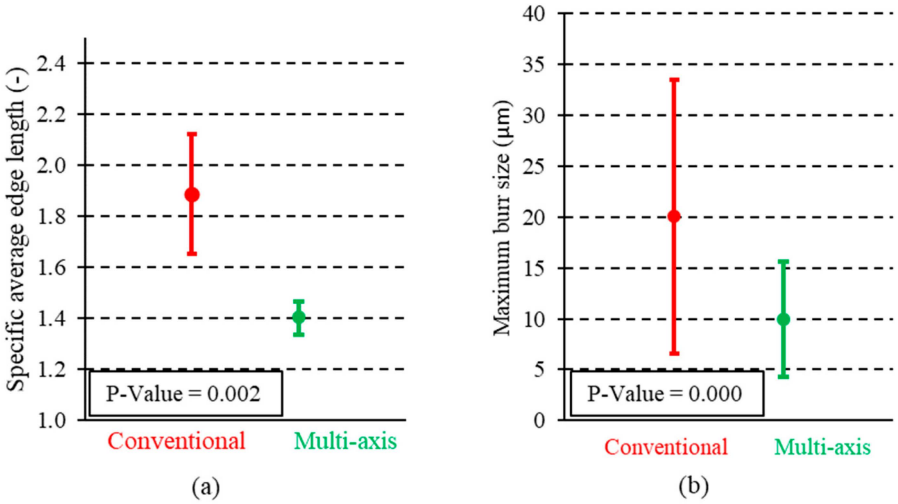

Figure 9. The main effect diagram of the machining technologies: (**a**) specific average edge length (L_e) and (**b**) maximum burr size (L_b).

Table 4. ANOVA tables for (a) the specific average edge length and (b) the maximum burr size, where bold entries denote *p*-values lower than 0.05, indicating that the particular factor has a significant effect.

(a)		**(b)**	
L_e (-)		**L_b (µm)**	
Source	*p*-Value	Source	*p*-Value
Model	0.063	Model	0.003
Linear	0.014	Linear	0.000
v_f (mm/min)	0.241	v_f (mm/min)	0.669
a_e (mm)	0.936	a_e (mm)	0.307
T (-)	**0.002**	T (-)	**0.000**
Square	0.592	Square	0.699
v_f (mm/min) · v_f (mm/min)	0.641	v_f (mm/min) · v_f (mm/min)	0.548
a_e (mm) · a_e (mm)	0.342	a_e (mm) · a_e (mm)	0.511
2-Way Interaction	0.309	2-Way Interaction	0.457
v_f (mm/min) · a_e (mm)	0.110	v_f (mm/min) · a_e (mm)	0.233
v_f (mm/min) · T (-)	0.379	v_f (mm/min) · T (-)	0.943
a_e (mm) · T (-)	0.647	a_e (mm) · T (-)	0.290

Figure 10a shows the specific average edge length values of each experimental setting. Figure 10a shows that the specific average edge length was larger in almost all cases for edges machined with conventional technology. The largest difference was seen in the fourth experimental setting, where the difference was 1.296. The second most significant difference was in the second experimental setting, where the difference was 0.886. As shown in Figure 10a, slight differences existed in the fifth (0.005), ninth (0.011) and eleventh (0.03) experimental settings. In the ninth experimental setting, the specific average edge length was smaller when machining was performed with conventional technology. The possible reason for this is that the factors set in the ninth trial of machining with conventional technology approach the ideal machining parameters of conventional technology. More considerable differences can be seen when the maximum burr size is plotted for each experimental setting, as depicted in Figure 10b. The only exception was found in the second experimental setting for the maximum burr size, shown in Figure 10b.

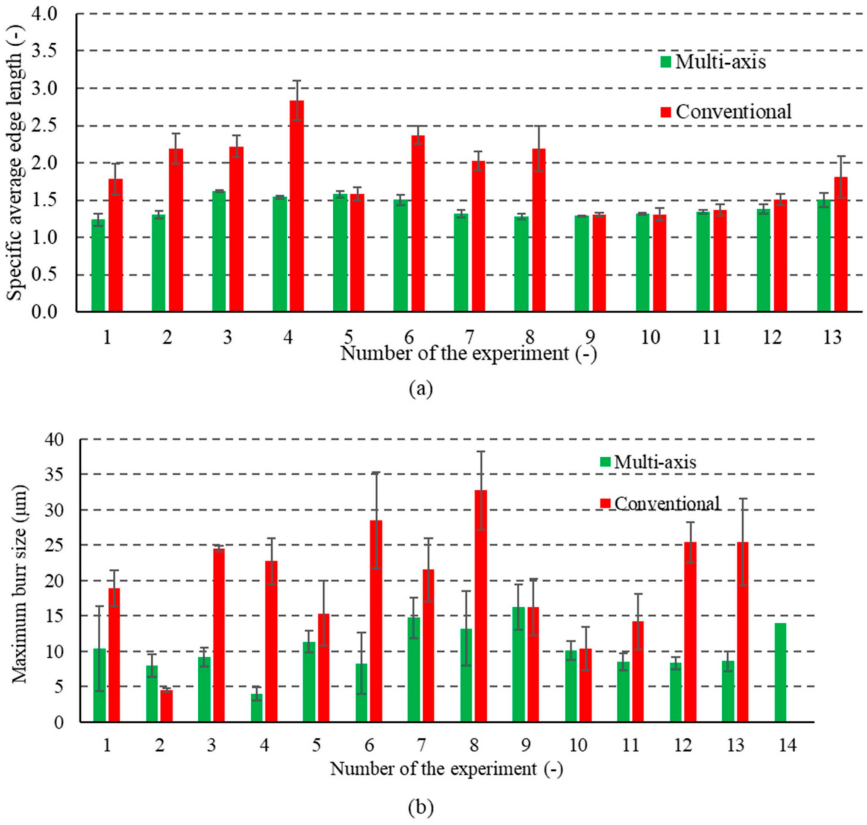

Figure 10. Red represents the CFRP plate machined by conventional technology, and green represents the CFRP plate machined by multi-axis technology. (**a**) The specific average edge length (L_e) of each experimental setting. (**b**) The maximum burr size (L_b) of each experimental setting.

As shown in Figure 11a, a decreasing trend can be seen if the specific average edge length (L_e) is plotted as a function of feed rate (v_f). The specific average edge length achieved with multi-axis machining technology decreased to a lesser extent than that achieved with conventional machining technology. This means that we obtained more consistent results by machining with multi-axis technology. However, the means indicate that the larger the feed rate, the smaller the value of L_e; nonetheless, this effect cannot be considered significant according to the ANOVA table (Table 4a).

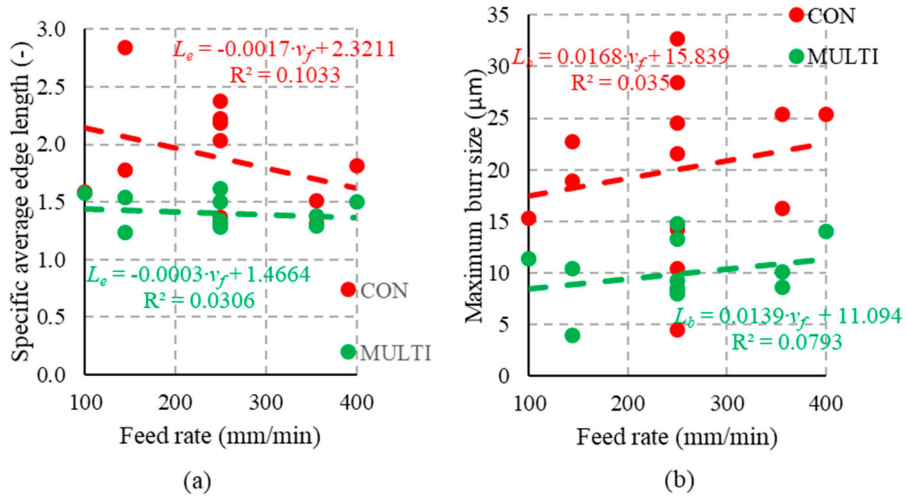

Figure 11. (**a**) Diagram of the specific average edge length (L_e) as a function of the feed rate (v_f); (**b**) diagram of the maximum burr size (L_b) as a function of the feed rate (v_f).

As depicted in Figure 12a, a decreasing trend can be seen in the case of edges made with multi-axis technology, while edges machined with conventional technology show an increasing trend if the specific average edge length (L_e) is plotted as a function of the cutting width (a_e). The specific average edge length of samples machined with multi-axis technology had a lower absolute slope than that of samples machined with conventional technology. This means that by using multi-axis technology, we obtained more even results. Larger differences can be seen when the maximum burr size is plotted as a function of the cutting width, as shown in Figure 12b. Although the expected values suggested the optimal conditions, the ANOVA showed that these effects were not significant; thus, a maximal feed rate is proposed for a greater material removal rate.

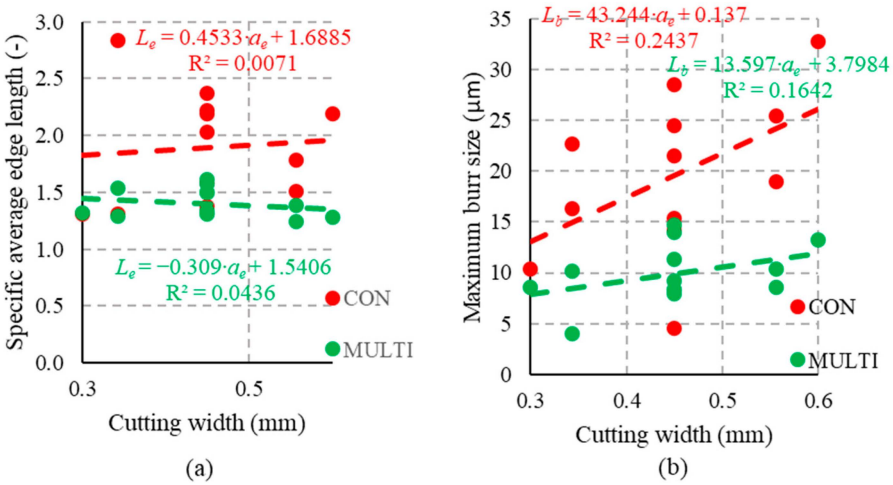

Figure 12. (**a**) Diagram of the specific average edge length (L_e) as a function of the cutting width (a_e); (**b**) diagram of the maximum burr size (L_b) as a function of the cutting width (a_e).

4.2. Influence of the Tool Tilting Angle and Permanent Chamfer Size

The experimental runs, the factor levels and the corresponding calculated response values (L_e and L_b) are summarised in Table 5. The raw images are illustrated in Figure 13.

Table 5. Experimental runs, factor levels and calculated response values.

Number of Experiments	Factors		Responses	
	Tool Tilting Angle	Permanent Chamfer Size	Specific Average Edge Length	Maximum Burr Size
No (-)	φ (°)	c (mm)	L_e (-)	L_b (µm)
1	143.934	0.556	1.779	18.929
2	143.934	0.556	1.239	10.407
3	250.000	0.450	2.195	4.496
4	250.000	0.450	1.309	7.986
5	250.000	0.450	2.219	24.507
6	250.000	0.450	1.617	9.207
7	143.934	0.343	2.837	22.729
8	143.934	0.343	1.541	3.999
9	100.000	0.450	1.584	15.343
10	100.000	0.450	1.579	11.379
11	250.000	0.450	2.371	28.495
12	250.000	0.450	1.503	8.309
13	250.000	0.450	2.031	21.538

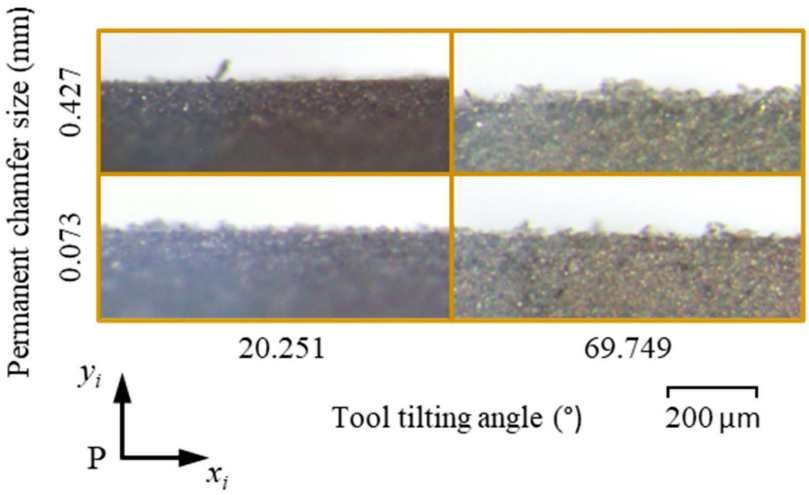

Figure 13. Raw images of the machined edges of the CFRP composites.

The ANOVA tables show a significant influence of the tool tilting angle on L_e and L_b; however, the permanent chamfer size was not relevant at a significance level of 0.05. The ANOVA tables are provided (Table 6).

Table 6. ANOVA tables for (a) the specific average edge length and (b) the maximum burr size, where bold entries denote *p*-values lower than 0.05, indicating that the particular factor has a significant effect.

(a)		**(b)**	
L_e (-)		**L_b (µm)**	
Source	*p*-Value	Source	*p*-Value
Model	0.001	Model	0.005
Linear	0.000	Linear	0.004
φ (°)	**0.000**	φ (°)	**0.001**
c (mm)	0.246	c (mm)	0.803
Square	0.003	Square	0.010
φ (°) · φ (°)	**0.001**	φ (°) · φ (°)	**0.003**
c (mm) · c (mm)	0.060	c (mm) · c (mm)	0.382
2-Way Interaction	0.559	2-Way Interaction	0.210
φ (°) · c (mm)	0.559	φ (°) · c (mm)	0.210

As depicted in Figure 14a, we fitted a quadratic model to the data points, as this model's determination coefficient (0.8661) was significantly larger than the linear model's (0.6135). Even larger differences can be seen when the maximum burr size is plotted as a function of the tool tilting angle, as shown in Figure 14b. The ANOVA (Table 6) showed that the influence of the tool tilting angle on the machined edge quality was significant. It can be concluded that there is an optimal tool tilting angle that is beneficial from the point of view of minimising machining-induced burrs. That tool tilting angle is about 20 degrees.

Although the expected values suggest that larger permanent chamfer sizes are associated with slightly better-quality machined edges, the ANOVA (Table 6) showed that c did not have a significant influence on either L_b or L_e. Thus, the chamfer size is recommended to be set according to the particular application, which will not significantly influence the quality of the machined edges.

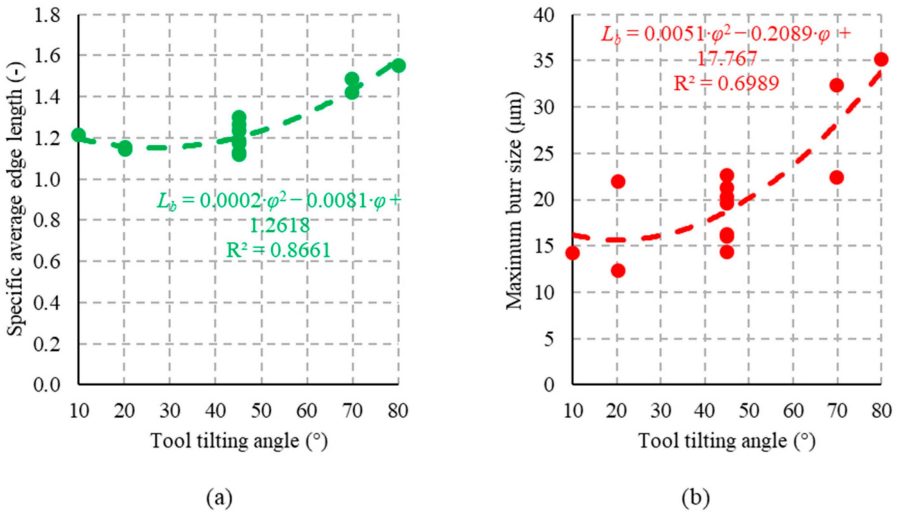

Figure 14. (**a**) Diagram of the specific average edge length (L_e.) as a function of the tool tilting angle (φ); (**b**) diagram of the maximum burr size (L_b) as a function of the tool tilting angle (φ).

4.3. Discussion and Outlook

The presented experimental results indicate that the developed multi-axis edge-trimming technology is more beneficial than the conventional technology from the point of view of machining-induced burr formation. Although the measured burr sizes were very small for both technologies and may not make the assembly of such machined composite parts difficult, small burrs also have the potential to become starting locations for delamination, lowering the resultant load-bearing capacity [5]. Therefore, the minimisation of burr formation is essential. Furthermore, it has to be highlighted that the condition of the cutting tool applied in this study was fresh (i.e., not worn due to the minimal length of machining); thus, the burr was not as considerable even in the case of the conventional technology. However, if the tool condition changes significantly, the increased cutting edge radius is expected to result in more burrs in conventional machining [12,38]. Considering that the compression effect of the multi-axis edge trimming technology is expected to allow even a worn cutting tool to produce high-quality edges on CFRPs, we conducted trials to prove it. A two-fluted, worn HSS end mill having a diameter of 6 mm and a nominal flank wear of 60 µm was applied for the edge-trimming trials. The cutting tool is shown in Figure 15. The quality of the machined edges was similarly photographed and evaluated through digital image processing, as presented in Section 3. Figure 16 shows representative segmented images that clearly indicate that the maximum burr size (830 µm) is comparable to the width of the cut in the case of the conventional technology (Figure 16b); however, it is significantly smaller (76 µm) in the case of the multi-axis technology (Figure 16a). This suggests that the relevancy of the multi-axis technology comes to the fore if the tool condition significantly changes. For example, the edge of a composite part may be machined using conventional edge trimming until the considerable tool wear results in an unaccepted burr size; then, the technology may be changed to the multi-axis one to maintain a high-quality edge.

We also examined the quality of edges machined by the worn cutting tool using scanning electron microscopy (SEM). Representative images are shown in Figure 17. The difference in the machining technology is clearly visible, as the edge and connected surfaces are smoother and follow the nominal edge geometry in the case of the multi-axis technology. The higher-magnification images also differ significantly, as the presence of the polymer matrix differs. The fractured fibres are well supported by the cut matrix when the multi-axis technology is applied; however, the conventional technology seems to peel off the matrix from the fibres, resulting in less material continuity and resultant strength. The SEM images also prove the relevancy of the novel multi-axis technology.

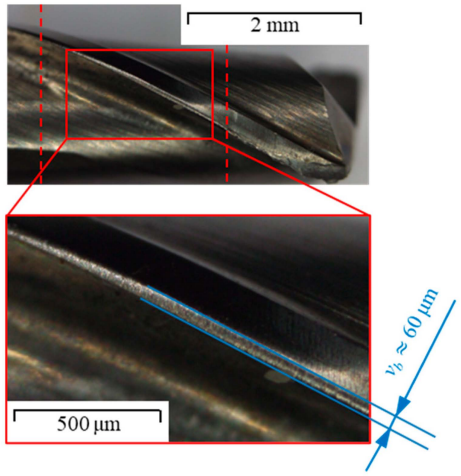

Figure 15. Microscopic image of the applied worn tool from a radial direction, where v_b (µm) is the nominal flank wear.

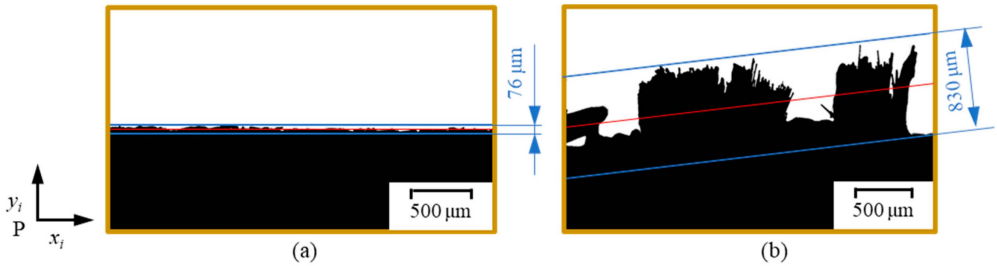

Figure 16. The difference between the two technologies using a worn tool: (**a**) multi-axis technology and (**b**) conventional technology.

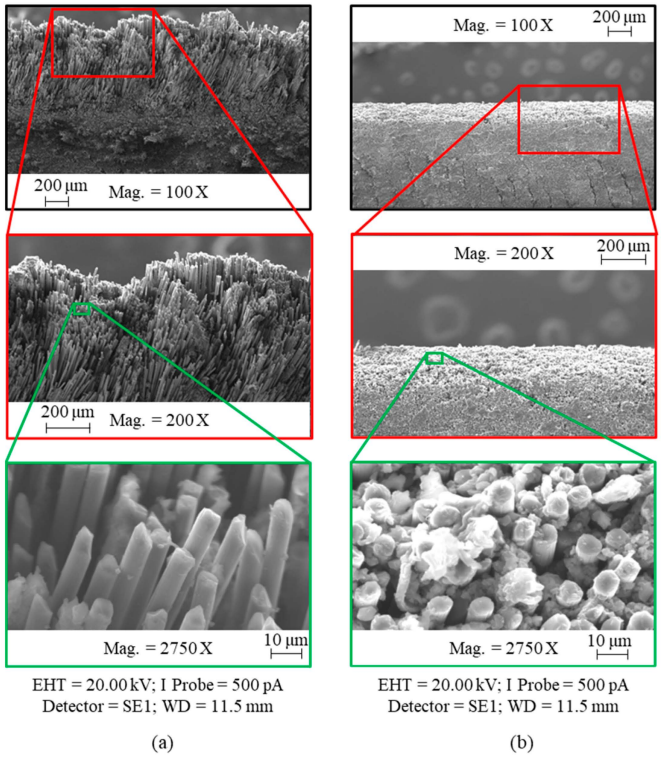

Figure 17. SEM images of edges machined using a low-grade tool and (**a**) conventional technology or (**b**) multi-axis technology.

The analysed quality parameters (L_b and L_e from Table 3) were visualized as a scatter plot to further discuss the findings, as can be seen in Figure 18. This diagram confirms the achievability of good-quality edges machined by the developed technology because the resultant points are positioned in two significantly different regions. While the multi-axial parameters are located in Region B, the conventional ones are located in Region A. These regions differ in position and size; in particular, the size difference suggests that multi-axis technology is more controllable than conventional technology, as the quality parameters are closer to each other than in the case of conventional technology.

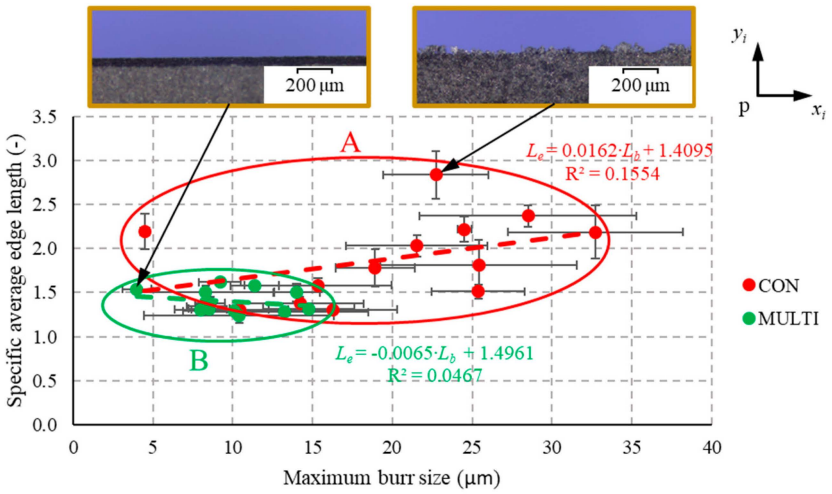

Figure 18. Scatter plot of maximum burr size and specific average edge length in the cases of conventional (CON) and multi-axis (MULTI) technologies.

The quality of the multi-axis-machined edges exceeded that of the conventionally machined edges in all the selected factor levels; the implementation and optimisation of this technology are recommended in the future so that it can attract significant industrial interest. Other significant aspects of the spread of the multi-axis edge-trimming technology are the material removal rate (MRR) and machining time (t_m), which need to be discussed. The ratio of the MRR of the multi-axis technology to that of the conventional technology can be calculated as expressed by Equations (5)–(8).

$$\frac{MRR_{multi-axis,\ i}}{MRR_{conventional,\ i}} = \frac{((i-1)\cdot A_{IV} + A_I + A_{II} + A_{III})\cdot v_f}{i\cdot A_{IV}\cdot v_f} \tag{5}$$

$$A_{IV} = a_{ef}\cdot s \tag{6}$$

$$A_I = \frac{1}{2}tg(\varphi_1)\cdot\left(c + a_{ef}\right)^2,\ \ A_{II} = \frac{1}{2}tg(\varphi_2)\cdot\left(c + a_{ef}\right)^2 \tag{7}$$

$$A_{III} = \frac{1}{2}a_{ef}^2\cdot tg(\varphi_1) + \frac{1}{2}a_{ef}^2\cdot tg(\varphi_2) + (s - 2\cdot tg(\varphi)\cdot(c + a_{ef}))\cdot a_{ef} \tag{8}$$

where $MRR_{multi\text{-}axis,\ i}$ is the ith material removal rate of the multi-axis technology; $MRR_{conventional,\ i}$ is the ith material removal rate of the conventional technology; A_{IV} is the area that is removed with the conventional technology (shown in Figure 4b); A_I and A_{II} are the areas that are removed with the multi-axis technology in the first and second steps, respectively (area I (triangle AEB) and area II (triangle A'E'B'), as shown in Figure 2); A_{III} is the area that is removed with the multi-axis technology in the final step (area III (quadrilateral BDD'B'), as shown in Figure 2); v_f is the feed rate; a_{ef} is the cutting width in the final step; s is the width of the CFRP plate; φ is the tool tilting angle and c is the permanent chamfer size. If the number of grips is increasing, the MRR of the ratio approaches one, i.e.,

the greater the number of grips, the closer the MMR of the technologies, as expressed by Equation (9) and illustrated in Figure 19a.

$$\lim_{i \to \infty} \frac{MRR_{multi-axis,\ i}}{MRR_{conventional,\ i}} = 1 \tag{9}$$

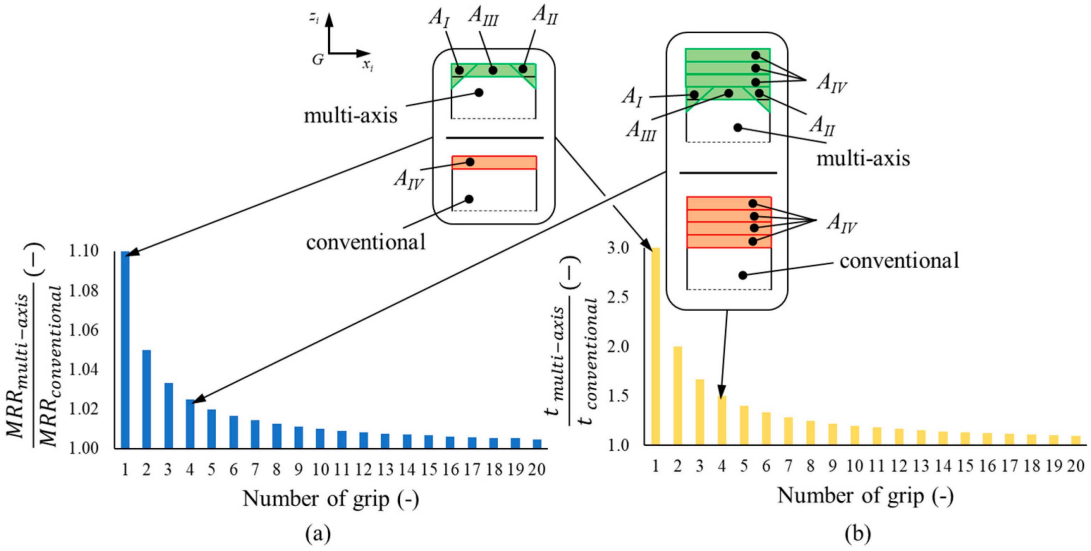

Figure 19. Illustration of the influence of the number grips on the (**a**) ratio of MRR and (**b**) ratio of machining time.

As with the MRR, the difference in the machining time of the technologies becomes smaller as the number of grips increases, as illustrated in Figure 19b. This suggests that the multi-axis edge trimming technology is even more competitive if the material allowance to be removed requires more grips.

It is worth highlighting that the three grips of the multi-axis edge trimming technology cannot be considered conventional roughing, pre-finishing and finishing passes, as the compression effect of the conventional helical end mill here is not provided. Furthermore, the feeds investigated were the same for both technologies due to considerations regarding the design of experiments (DoE). Therefore, the differences in the chip cross-sections could not be considered in this experimental work. Therefore, the feed rate of the particular passes must fit the chip cross-sections and aims of particular passes in the future. This may result in an even higher feed rate in the three passes, significantly increasing the MRR, thus pushing this technology closer to a higher technology readiness level.

5. Conclusions

The present study introduced a novel multi-axis edge-trimming technology for high-quality edge trimming of fibrous polymer composites. The efficiency of the novel technology was experimentally analysed and compared with results from conventional edge milling. Based on this study, the following conclusions can be drawn.

The study introduced a novel multi-axis edge-trimming technology that is inspired by the wobble milling of holes in FRPs. The FRP composite edge is machined in three passes using a conventional end mill. First, chamfers are machined to compress the outer layers and minimise machining-induced burr formation by a compression effect. The rest of the material is then removed by conventional helical milling. The final edge of the FRP part is high-quality even with significantly changed tool conditions.

The ANOVA results show that the edges machined by the multi-axis edge-trimming technology are significantly better in quality than the edges machined by the conventional technology. However, neither the permanent chamfer size nor the feed rate nor the cutting width has a significant influence on the burr characteristics at a significance level of 0.05.

The ANOVA results prove that the selection of the proper tilting angle is crucial, as the tool tilting angle has a significant influence on the burr characteristics. The optimal tool tilting condition was found to be around 22° in this study.

This industrial implementation of the introduced multi-axis edge-trimming technology requires further research and development in the following areas: (i) increasing the material removal rate and decreasing the machining time, (ii) determining the trigger value at which to change from the conventional technology to the multi-axis technology, (iii) conducting a detailed analysis of the influences of the cutting speed, tool condition and helix angle of the cutting tool and (iv) determining the minimal curvature to be machined considering the composite plate's thickness, the material allowance and the tool geometry.

Author Contributions: Conceptualization, N.G. and T.S.T.; methodology, N.G.; software, T.S.T.; validation, T.S.T.; formal analysis, T.S.T.; investigation, N.G. and T.S.T.; data curation, T.S.T.; writing—original draft, T.S.T.; writing—review and editing, N.G.; visualization, T.S.T.; supervision, N.G. All authors have read and agreed to the published version of the manuscript.

Funding: This research was partly supported by the János Bolyai Research Scholarship of the Hungarian Academy of Sciences No. BO/00508/22/6 and by the Ministry of Culture and Innovation of Hungary from the National Research, Development and Innovation Fund, financed under the EKÖP-24-3-BME-335 and EKÖP-24-4-II-BME-157 funding scheme. The authors acknowledge the support of Dániel István Poór and Péter János Szabó in the experimental work.

Data Availability Statement: Data from the experiments carried out may be shared on request.

Conflicts of Interest: The authors declare no conflict of interest.

References

1. Lee, S.-C.; Jeong, S.-T.; Park, J.-N.; Kim, S.-J.; Cho, G.-J. Study on Drilling Characteristics and Mechanical Properties of CFRP Composites. *Acta Mech. Solida Sin.* **2008**, *21*, 364–368. [CrossRef]
2. Takacs, L.; Szabó, F. Automated Determination of the Optimal Manufacturing Direction of Polymer Composite Shell Structures. *IOP Conf. Ser. Mater. Sci. Eng.* **2022**, *1246*, 012026. [CrossRef]
3. Teti, R. Machining of Composite Materials. *CIRP Ann.* **2002**, *51*, 611–634. [CrossRef]
4. Bernasconi, A.; Cosmi, F.; Dreossi, D. Local Anisotropy Analysis of Injection Moulded Fibre Reinforced Polymer Composites. *Compos. Sci. Technol.* **2008**, *68*, 2574–2581. [CrossRef]
5. Poór, D.I.; Geier, N.; Pereszlai, C.; Xu, J. A Critical Review of the Drilling of CFRP Composites: Burr Formation, Characterisation and Challenges. *Compos. Part B Eng.* **2021**, *223*, 109155. [CrossRef]
6. Dornfeld, D.; Min, S. A Review of Burr Formation in Machining. In *Burrs-Analysis, Control and Removal, Proceedings of the CIRP International Conference on Burrs, Kaiserslautern, Germany, 2–3 April 2009*; Springer: Berlin/Heidelberg, Germany, 2010; pp. 3–11, ISBN 978-3-642-00567-1.
7. Park, K.M.; Kurniawan, R.; Yu, Z.; Ko, T.J. Evaluation of a Hybrid Cryogenic Deburring Method to Remove Uncut Fibers on Carbon Fiber-Reinforced Plastic Composites. *Int. J. Adv. Manuf. Technol.* **2019**, *101*, 1509–1523. [CrossRef]
8. Gaugel, S.; Sripathy, P.; Haeger, A.; Meinhard, D.; Bernthaler, T.; Lissek, F.; Kaufeld, M.; Knoblauch, V.; Schneider, G. A Comparative Study on Tool Wear and Laminate Damage in Drilling of Carbon-Fiber Reinforced Polymers (CFRP). *Compos. Struct.* **2016**, *155*, 173–183. [CrossRef]
9. Voß, R.; Henerichs, M.; Rupp, S.; Kuster, F.; Wegener, K. Evaluation of Bore Exit Quality for Fibre Reinforced Plastics Including Delamination and Uncut Fibres. *CIRP J. Manuf. Sci. Technol.* **2016**, *12*, 56–66. [CrossRef]
10. Geier, N.; Xu, J.; Poór, D.I.; Dege, J.H.; Davim, J.P. A Review on Advanced Cutting Tools and Technologies for Edge Trimming of Carbon Fibre Reinforced Polymer (CFRP) Composites. *Compos. Part B Eng.* **2023**, *266*, 111037. [CrossRef]
11. Cunningham, C.R.; Shokrani, A.; Dhokia, V. Edge Trimming of Carbon Fibre Reinforced Plastic. *Procedia CIRP* **2018**, *77*, 199–202. [CrossRef]
12. Jin, F.; Bao, Y.; Li, B.; Jin, X. Tool Wear Prediction in Edge Trimming of Carbon Fiber Reinforced Polymer Using Machine Learning with Instantaneous Parameters. *J. Manuf. Process.* **2022**, *82*, 277–295. [CrossRef]
13. El-Hofy, M.; Helmy, M.O.; Escobar-Palafox, G.; Kerrigan, K.; Scaife, R.; El-Hofy, H. Abrasive Water Jet Machining of Multidirectional CFRP Laminates. *Procedia CIRP* **2018**, *68*, 535–540. [CrossRef]
14. El-Hofy, M.H.; El-Hofy, H. Laser Beam Machining of Carbon Fiber Reinforced Composites: A Review. *Int. J. Adv. Manuf. Technol.* **2019**, *101*, 2965–2975. [CrossRef]
15. Guu, Y.H.; Hocheng, H.; Tai, N.H.; Liu, S.Y. Effect of Electrical Discharge Machining on the Characteristics of Carbon Fiber Reinforced Carbon Composites. *J. Mater. Sci.* **2001**, *36*, 2037–2043. [CrossRef]

16. Hintze, W.; Cordes, M.; Geis, T.; Blühm, M.; Emmelmann, C.; Canisius, M. Laser Scored Machining of Fiber Reinforced Plastics to Prevent Delamination. *Procedia Manuf.* **2016**, *6*, 1–8. [CrossRef]
17. Wang, F.; Yin, J.; Ma, J.; Jia, Z.; Yang, F.; Niu, B. Effects of Cutting Edge Radius and Fiber Cutting Angle on the Cutting-Induced Surface Damage in Machining of Unidirectional CFRP Composite Laminates. *Int. J. Adv. Manuf. Technol.* **2017**, *91*, 3107–3120. [CrossRef]
18. Su, Y.; Jia, Z.; Niu, B.; Bi, G. Size Effect of Depth of Cut on Chip Formation Mechanism in Machining of CFRP. *Compos. Struct.* **2017**, *164*, 316–327. [CrossRef]
19. Schorník, V.; Daňa, M.; Zetková, I. The Influence of the Cutting Conditions on the Machined Surface Quality When the CFRP Is Machined. *Procedia Eng.* **2015**, *100*, 1270–1276. [CrossRef]
20. Pecat, O.; Rentsch, R.; Brinksmeier, E. Influence of Milling Process Parameters on the Surface Integrity of CFRP. *Procedia CIRP* **2012**, *1*, 466–470. [CrossRef]
21. Yashiro, T.; Ogawa, T.; Sasahara, H. Temperature Measurement of Cutting Tool and Machined Surface Layer in Milling of CFRP. *Int. J. Mach. Tools Manuf.* **2013**, *70*, 63–69. [CrossRef]
22. Geier, N. Influence of Fibre Orientation on Cutting Force in up and down Milling of UD-CFRP Composites. *Int. J. Adv. Manuf. Technol.* **2020**, *111*, 881–893. [CrossRef]
23. Liu, C.; Ren, J.; Shi, K.; Zhang, Y. Investigation of Fracture Mechanism Evolution Model for UD-CFRP and MD-CFRP during the Milling Process. *Compos. Struct.* **2023**, *306*, 116585. [CrossRef]
24. Zhang, L.; Zhang, X. A Comparative Experimental Study of Unidirectional CFRP High-Speed Milling in up and down Milling with Varied Angles. *J. Manuf. Process.* **2023**, *101*, 1147–1157. [CrossRef]
25. Jia, Z.; Rao, F.; Fuji, W.; Qian, B.; Chunling, H. Temperature Effects in End Milling Carbon Fiber Reinforced Polymer Composites. *Polym. Compos.* **2016**, *39*, 437–447. [CrossRef]
26. Li, Y.; Wang, F.; Zhang, B.; Deng, J.; Fu, R.; He, Q.; Ma, X. A Novel Discrete-Edge Ball End Milling Cutter: Suitable for Milling Weakly Rigid Curved CFRP Parts. *J. Mater. Process. Technol.* **2023**, *317*, 117996. [CrossRef]
27. Sheikh-Ahmad, J.; El-Hofy, M.; Almaskari, F.; Kerrigan, K.; Takikawa, Y. The Evolution of Cutting Forces during Slot Milling of Unidirectional Carbon Fiber Reinforced Polymer (UD-CFRP) Composites. *Procedia CIRP* **2019**, *85*, 127–132. [CrossRef]
28. El-Hofy, M.H.; Soo, S.L.; Aspinwall, D.K.; Sim, W.M.; Pearson, D.; M'Saoubi, R.; Harden, P. Tool Temperature in Slotting of CFRP Composites. *Procedia Manuf.* **2017**, *10*, 371–381. [CrossRef]
29. Xu, Z.; Wang, Y. Study on Milling Force and Surface Quality during Slot Milling of Plain-Woven CFRP with PCD Tools. *Materials* **2022**, *15*, 3862. [CrossRef]
30. Ning, H.; Zheng, H.; Yuan, X. Establishment of Instantaneous Milling Force Prediction Model for Multi-Directional CFRP Laminate. *Adv. Mech. Eng.* **2021**, *13*. [CrossRef]
31. Zhang, J.; Huang, X.; Kang, X.; Yi, H.; Wang, Q.; Cao, H. Energy Field-Assisted High-Speed Dry Milling Green Machining Technology for Difficult-to-Machine Metal Materials. *Front. Mech. Eng.* **2023**, *18*, 28. [CrossRef]
32. Chen, X.; Zhang, Y.; Li, A. Laser Processing and Multi-Energy Field Manufacturing of High-Performance Materials. *Materials* **2023**, *16*, 5991. [CrossRef] [PubMed]
33. Jiao, J.; Cheng, X.; Wang, J.; Sheng, L.; Zhang, Y.; Xu, J.; Jing, C.; Sun, S.; Xia, H.; Ru, H. A Review of Research Progress on Machining Carbon Fiber-Reinforced Composites with Lasers. *Micromachines* **2023**, *14*, 24. [CrossRef] [PubMed]
34. Zenia, S.; Ben Ayed, L.; Nouari, M.; Delamézière, A. Numerical Analysis of the Interaction between the Cutting Forces, Induced Cutting Damage, and Machining Parameters of CFRP Composites. *Int. J. Adv. Manuf. Technol.* **2015**, *78*, 465–480. [CrossRef]
35. Kerrigan, K.; Scaife, R.J. Wet vs Dry CFRP Drilling: Influence of Cutting Fluid on Tool Performance. *Procedia CIRP* **2018**, *77*, 315–319. [CrossRef]
36. Gunaraj, L.; Paul, S.; Mohammed, J.; Sudhagar, E.; Thankachan, T. Optimization of Cutting Parameters for Hard Boring of AISI 4340 Steel Using Signal-to-Noise Ratio, Grey Relation Analysis and Analysis of Variance. *Period. Polytech. Mech. Eng.* **2023**, *67*, 259–269. [CrossRef]
37. Geier, N.; Szalay, T.; Biró, I. Trochoid Milling of Carbon Fibre-Reinforced Plastics (CFRP). *Procedia CIRP* **2018**, *77*, 375–378. [CrossRef]
38. Póka, G.; Balázs, B.Z. A Robust Digital Image Processing Method for Measuring the Planar Burr Length at Milling. *J. Manuf. Process.* **2022**, *80*, 706–717. [CrossRef]
39. Balázs, B.Z.; Takács, M. Experimental Investigation of Surface Characteristics and Dynamic Effects at Micro Milling of Hardened Hot-Work Tool Steel. *Int. J. Mach. Mach. Mater.* **2020**, *22*, 504–526. [CrossRef]
40. Sun, Z.; Geng, D.; Zheng, W.; Liu, Y.; Liu, L.; Ying, E.; Jiang, X.; Zhang, D. An Innovative Study on High-Performance Milling of Carbon Fiber Reinforced Plastic by Combining Ultrasonic Vibration Assistance and Optimized Tool Structures. *J. Mater. Res. Technol.* **2023**, *22*, 2131–2146. [CrossRef]
41. Pereszlai, C.; Geier, N.; Poór, D.I.; Balázs, B.Z.; Póka, G. Drilling Fibre Reinforced Polymer Composites (CFRP and GFRP): An Analysis of the Cutting Force of the Tilted Helical Milling Process. *Compos. Struct.* **2021**, *262*, 113646. [CrossRef]
42. Hosokawa, A.; Hirose, N.; Ueda, T.; Furumoto, T. High-Quality Machining of CFRP with High Helix End Mill. *CIRP Ann.* **2014**, *63*, 89–92. [CrossRef]
43. Schulze, V.; Spomer, W.; Becke, C. A Voxel-Based Kinematic Simulation Model for Force Analyses of Complex Milling Operations Such as Wobble Milling. *Prod. Eng.* **2012**, *6*, 1–9. [CrossRef]

44. Schulze, V.; Becke, C.; Weidenmann, K.; Dietrich, S. Machining Strategies for Hole Making in Composites with Minimal Workpiece Damage by Directing the Process Forces Inwards. *J. Mater. Process. Technol.* **2011**, *211*, 329–338. [CrossRef]
45. Hintze, W.; Brügmann, F. Influence of Spatial Tool Inclination on Delamination When Milling CFRP. *J. Mater. Process. Technol.* **2018**, *252*, 830–837. [CrossRef]
46. Pereszlai, C.; Geier, N. Comparative Analysis of Wobble Milling, Helical Milling and Conventional Drilling of CFRPs. *Int. J. Adv. Manuf. Technol.* **2020**, *106*, 3913–3930. [CrossRef]
47. Geier, N.; Szalay, T.; Takács, M. Analysis of Thrust Force and Characteristics of Uncut Fibres at Non-Conventional Oriented Drilling of Unidirectional Carbon Fibre-Reinforced Plastic (UD-CFRP) Composite Laminates. *Int. J. Adv. Manuf. Technol.* **2019**, *100*, 3139–3154. [CrossRef]